Received: 4 August 2021 | Revised: 5 November 2021 | Accepted: 3 December 2021

IET Optoelectronics

DOI: 10.1049/ote2.12063

The Institution of Engineering and Technology WILEY

ORIGINAL RESEARCH

Ultra-compact and ultra-broadband hybrid plasmonic-photonic vertical coupler with high coupling efficiency, directivity, and polarisation extinction ratio

Hamed Pezeshki[1,2] | Amanda J. Wright[1] | Eric C. Larkins[1]

[1]Optics and Photonics Research Group, Faculty of Engineering, University of Nottingham, Nottingham, UK

[2]Department of Applied Physics, Eindhoven University of Technology, Eindhoven, The Netherlands

Correspondence

Eric C. Larkins, Optics and Photonics Research Group, Faculty of Engineering, University Park, Nottingham, NG7 2RD, UK.
Email: eric.larkins@nottingham.ac.uk

Funding information

Engineering and Physical Sciences Research Council, Grant/Award Number: EP/R025282/1

Abstract

An ultra-compact, ultra-broadband vertical coupler for dense photonic integrated circuits is reported with a 1.07 × 0.62 μm^2 wavelength-scale footprint. This hybrid plasmonic-photonic coupler uses a unique two-plane plasmonic nanoantenna array on a silicon-on-insulator waveguide. The in- and out-of-plane interference of the multipole moments and dual-feed nanoantennas results in efficient, unidirectional coupling. Finite-element simulations show that, for a 0.8 μm diameter Gaussian beam, the maximum coupling efficiency (CE) is −3.4 dB across the telecommunication C-, L- and U-bands with a 3-dB bandwidth of 230 nm. The CE is > 9 dB higher than recently reported ultra-compact plasmonic couplers. The maximum directivity and polarisation extinction ratio across the C- to U-bands are 9.2 and 24.1 dB, respectively. Finally, as an out-coupler, it has a vertical directivity of >8.5 dB, enabling its use for vertical optical interconnects between two vertically separated circuits.

KEYWORDS

plasmonics, surface plasmon resonance

1 | INTRODUCTION

Optical couplers are used extensively for telecommunication applications as a component to couple light into photonic integrated circuits (PICs). Due to the nanoscale cross section of waveguides in PICs (e.g. photonic wires), miniaturisation and coupling efficiency (CE) are two main challenges when designing optical couplers. Conventional edge couplers (ECs) [1] and vertical couplers (VCs) [2, 3] provide high CE but at the expense of miniaturisation and packing density. Plasmonic couplers (PCs) [4] can overcome the size challenge of conventional couplers but often suffer high absorption loss and require additional coupling to dielectric waveguides. This work reports on the design of a hybrid plasmonic-photonic vertical coupler (HVC) with an ultra-compact footprint and one-step dielectric waveguide coupling. This VC is based on a unique two-plane plasmonic nanoantenna (PNA) array (2P-NA) with a wavelength-scale footprint. The key innovations of our device compared to conventional Yagi-Uda antennas [5–11] are the use of dual-feed elements and in- and out-of-plane constructive interference of the electric dipole, electric quadrupole, and magnetic dipole moments of the 2P-NAs elements. These innovations provide strong CE, high directivity (D), large polarisation extinction ratio (PER) and ultra-broadband operation—making our device attractive for both telecommunications and other integrated ultra-broadband applications (e.g. Raman spectroscopy).

Silicon-on-insulator (SOI) is a popular platform for PICs as it can be used to fabricate low-cost large-scale PICs and is compatible with complementary metal-oxide-semiconductor (CMOS) technology [12–15]. For some telecommunication applications, the ability to integrate laser diodes gives InP-based PICs an advantage over other materials. For some biophotonic applications, Si_xN_y PICs are preferred for their low absorption losses at visible wavelengths. While the proposed device is suitable for all these platforms, SOI was chosen for compatibility with CMOS and its low cytotoxicity compared to GaAs for biophotonics applications.

The high refractive index contrast ($\Delta n \cong 2$) between the silicon (Si) waveguide and the silica (SiO_2) substrate of a SOI waveguide results in single-mode waveguides with a nanoscale cross section, for example, 500 nm width × 220 nm height, in the telecommunication C- to U-bands (1.530–1.675 μm). The high index contrast and small waveguide size allow the waveguides and components in PICs to be packed more densely but the nanoscale waveguide cross section makes it difficult to efficiently couple light from a laser or single-mode optical fibre (SMF) into the SOI waveguide. The mode field diameter (MFD) of an SMF (e.g. ~10.4 μm at a wavelength of 1.55 μm for Corning®SMF28®) is much larger than the MFD of a single-mode SOI waveguide (typically 0.5 μm), leading to large MFD mismatch and low optical CE. Optical couplers designed to address this mode mismatch can be categorised as ECs or VCs, according to their coupling geometry [1–3]. Edge couplers and VCs each have their advantages and disadvantages. Edge couplers are usually based on the adiabatic reduction of the mode profile of an SMF until it matches the mode profile of the single-mode waveguide. Edge couplers are broadband with a high CE but are comparatively long and need to be positioned at the edge of the chip.

Grating couplers (GCs), the most common type of VC, are based on surface diffraction gratings. They benefit from enhanced alignment tolerance, compatibility with wafer-scale fabrication and testing [2, 16], and the ability to couple light into the centre of a PIC. Vertical coupling adds great flexibility to the design of a PIC and eliminates the restriction on the number of couplers imposed on ECs by the chip circumference. It also facilitates wafer-scale testing of PICs before dicing and packaging. However, GCs must be as large as the MFD of an SMF and require a focussing grating and/or a long linear taper to connect to a single-mode SOI waveguide—adding to their size and complexity [16]. Focussing gratings require accurate alignment of the fibre position and angle and the linear tapers can cause strong back reflections [17]. The GC size can be reduced by illuminating it with a more tightly focussed beam but at the expense of reduced overall CE [17, 18]. Grating couplers are often narrowband (<100-nm bandwidth) and two-sided out-of-plane coupling restricts their CE. While their CE can be improved by using reflectors beneath the substrate, this increases their complexity and fabrication cost. Finally, fibres often require non-vertical coupling to fulfil the wave vector matching condition [19] and avoid strong second-order diffraction [17].

For a comprehensive review of Si-based couplers, interested readers are referred to [16, 17, 20]. Despite CE improvements, the large size of conventional ECs and VCs (>60 μm^2) impedes the realisation of ultra-compact PICs and introduces phase stability and latency issues that may affect the performance of coherent combining, phased arrays, and ultrafast circuits. Ultra-compact and ultra-broadband couplers are especially important for applications in densely packed PICs such as co-integration with very-large-scale integrated (VLSI) electronic circuits.

Plasmonic couplers, a type of VC based on plasmonic devices, are receiving increasing interest. Plasmonic couplers employ surface plasmon polaritons or localised surface plasmon resonances to overcome the diffraction limit of light, enabling the realisation of ultra-compact devices with micron- and nanometre-scale footprints [4]. Plasmonic couplers are simple to fabricate and overcome the size issues of conventional ECs and VCs but many PCs couple to plasmonic waveguides and suffer from high absorption losses due to large metal surfaces. These high absorption losses can lead to Joule heating and affect the functionality of nearby temperature-dependent devices–particularly, those employing micro- and nanoresonators. Plasmonic waveguides also suffer from much higher propagation losses (70 dB/mm [21]) than SOI ridge waveguides (0.24 ~ 0.36 dB/mm [22, 23]), and require coupling to SOI waveguides, which introduces an additional coupling loss of 1.5 to 4.5 dB [24, 25]. On the other hand, PNAs are able to address these losses by reducing the absorption cross section. Plasmonic nanoantennas based on the well-known configuration of the Yagi-Uda can also produce effective directional emission/reception, which is useful in cross-chip communications and directional single-photon sources [5–11], and biophotonics applications [26–28].

Recently, hybrid plasmonic-photonic couplers, created by coupling a PNA (array) to a photonic waveguide, eliminate the need for plasmonic-dielectric waveguide converters required by plasmonic waveguide-based PCs. While good progress has been made on in-plane hybrid couplers based on the Vivaldi antenna [29, 30], low-loss hybrid vertical plasmonic couplers (HVCs) remain challenging, due to the need for both a 90° change in the direction of the Poynting vector and unidirectional propagation. To date, HVCs have suffered from narrow bandwidth and very low CE of < -13 dB [31–35]. Table 1 compares the performance of recent HVCs, including the proposed 2P-NA HVC.

This paper presents a new class of HVC, that is, 2P-NA HVC, comprised of a 2P-NA coupled directly to a SOI waveguide. The performance of the 2P-NA HVC was simulated using COMSOL Multiphysics. For a Gaussian beam diameter of 0.8 μm, this 2P-NAs HVC has a 3-dB bandwidth of 230 nm, which expands to 300 nm for the 5-dB bandwidth (CE = −3.4 to −8.4 dB) to offer the ultra-broad wavelength operation from 1.530 to 1.830 μm. This coupler overcomes the problem of low CE while maintaining a miniaturised size of 1.07 × 0.62 μm^2, maximum D and PER of 9.2 and 24.1 dB, respectively. The CE represents an improvement of more than 9 dB when compared with the best recently reported HVCs [32–35]. Table 2 summarises the performance of the proposed 2P-NA HVC coupler. These benefits are achieved by the use of dual-feed elements in the two sets of antennas and the use of in- and out-of-plane constructive interference between the electric dipole, electric quadrupole, and magnetic dipole moments of the 2P-NAs elements. The proposed coupler can be used for coupling PICs to vertical-cavity surface-emitting laser (VCSEL) arrays [36–38] or as VCs and polarisation diversified power routers for telecommunication PICs. Unlike conventional ECs and VCs, this coupler has a comparable size to CMOS devices in VLSI circuits [39–41] (in contrast to ECs and VCs), making it a good candidate for cross-chip and board-to-board optical communication links (photonic-electronic convergence). Such links

TABLE 1 Performance overview at the peak coupling efficiency of recently reported plasmonic couplers and hybrid plasmonic-photonic vertical couplers, including the 2P-NA HVC proposed in this work

Coupler	Ref	Coupling efficiency (dB)	Directivity (dB)	Polarisation extinction ratio (dB)	Mode field diameter (μm)	Bandwidth (nm)	Size (μm^2)
PC	[32]	−13	5.5	n/a	2	n/a	0.73 × 0.5
	[33]	−16 CP	n/a	14	n/a	n/a	25 × 25
HVC	[34]	∼−13 TE^t	5	n/a	n/a	n/a	$\pi(0.2)^2 \times 0.6$
	[35]	−13 TE^t	13 TE^t	n/a	n/a	50 (3 dB)	0.36 × 0.6
		−14 TM^t	17.4 TM^t				
2P-NA HVC	***(This work)***	***−3.4 TE^t***	***7.7 TE^t***	***24.1 TE^t***	***0.8***	***230 (3 dB)***	***1.07 × 0.62***

Note: The superscript 't' stands for the theoretical results. The boldface font and italics was used to highlight the fact that this row of data referred to the work presented in this paper.
Abbreviations: HVC, hybrid vertical plasmonic-photonic coupler; PC, plasmonic coupler.

TABLE 2 Performance summary of the 2P-NA HVC for coupling efficiency ranges of: 3 dB (−3.4 to −6.4 dB); and 5 dB (−3.4 to −8.4 dB)

CE^t range (TE)	$D^t_{max(min)}$ (dB)	$PER^t_{max(min)}$ (dB)	BW^t (nm)	λ_{min}–λ_{max} (μm)
3 dB	9.2 (6.4)	24.1 (12.5)	230	1.56–1.79
5 dB	9.2 (6.4)	24.1 (7.7)	300	1.53–1.83

Note: t = theoretical.
Abbreviations: BW, bandwidth; CE, coupling efficiency; HVC, hybrid vertical plasmonic-photonic coupler; PER, polarisation extinction ratio.

could offer significant advantages over free-space optical interconnects [42] due to the small coupler size, the short in-plane optical path lengths, compatibility with CMOS fabrication and the elimination of vertical alignment and packaging issues. Moreover, the ultra-compact and ultra-broadband operation of 2P-NA HVC are attractive for ultra-broadband biophotonic applications such as two-photon fluorescence spectroscopy and surface-enhanced coherent-anti-Stokes Raman spectroscopy [43, 44].

2 | DESIGN OF HYBRID PLASMONIC-PHOTONIC VERTICAL COUPLER

This new coupler comprises a highly directional, ultra-compact (1.07 × 0.62 μm^2) 2P-NAs coupled to the evanescent field of the SOI waveguide. A Si ridge waveguide is placed on top of a 3-μm-thick (h_{sub}) buried-oxide-layer (BOX) SiO_2 substrate. The refractive indices used for the device design are based on the experimental data for SiO_2 and Si from Kischkat et al. [45] and Pierce et al. [46], respectively. The indices of the Au nanoantenna elements of the 2P-NA are taken from the experimental data of Johnson et al. [47]. The waveguide thickness, h_{co}, and width, w_{co}, were chosen to be 220 and 500 nm, respectively.

This coupler includes two NAs, NA-T and NA-B, placed at the top and bottom of the SOI waveguide, respectively. Each has dual-feed elements as the driving source and several director elements to give directivity to the electromagnetic wave. The reflector element reflects any residual backward scattered waves to the forward direction, that is, along the director elements [8]. In- and out-of-plane constructive interferences among the electric dipole, electric quadrupole, and magnetic dipole moments of the 2P-NA elements are used to reinforce a specific propagation direction inside the waveguide. Figure 1a shows a schematic diagram of the cross section of the 2P-NA HVC in the XZ plane, with excitation through the substrate, that is, from the bottom, and the intended propagation direction in the waveguide is along the X-axis.

Recently reported Yagi-Uda nanoantennas [5–11] have only used a one-feed element. In this work, dual-feed elements are introduced so that their driving fields add constructively. This increases the optical cross section of the 2P-NA and boosts its CE. Figure 1b presents a top view of the device in the XY plane at the top surface of the waveguide. The labels 'Directors-T' and 'Reflector-T' indicate that these elements belong to NA-T on the top surface of the waveguide. Note that all the antenna elements have the same width w_n and the Si waveguide has the width w_{co}. The layout of the second set of 2P-NAs is illustrated in Figure 1c, where the labels 'Directors-B' and 'Reflector-B' indicate that the elements belong to NA-B at the bottom of the waveguide. Both feed at the top and bottom surfaces of the waveguide have the same length l_f and gap width g_f. To achieve high CE, D, and PER across the 1.53–1.83 μm wavelength range, the dimensions of the 2P-NA are chosen to be g_f = 40 nm, $w_n = h_n$ = 30 nm, l_f = 290 nm, l_{r1} = 320 nm, l_{r2} = 350 nm, l_{d1} = 220 nm, l_{d2} = 195 nm, l_{d3} = 165 nm, l_{d4} = 115 nm, l_{d5} = 210 nm, $l_{d6} = l_{d7}$ = 200 nm, $S_f = S_{d2} = S_{d6}$ = 20 nm, S_{r1} = 570 nm, S_{r2} = 80 nm, S_{d1} = 200 nm, $S_{d3} = S_{d5} = S_{d7}$ = 40 nm, and S_{d4} = 60 nm.

The device dimensions and alignment tolerances are within the capabilities of modern electron beam lithography systems, now capable of writing sub-10 nm features. Indeed,

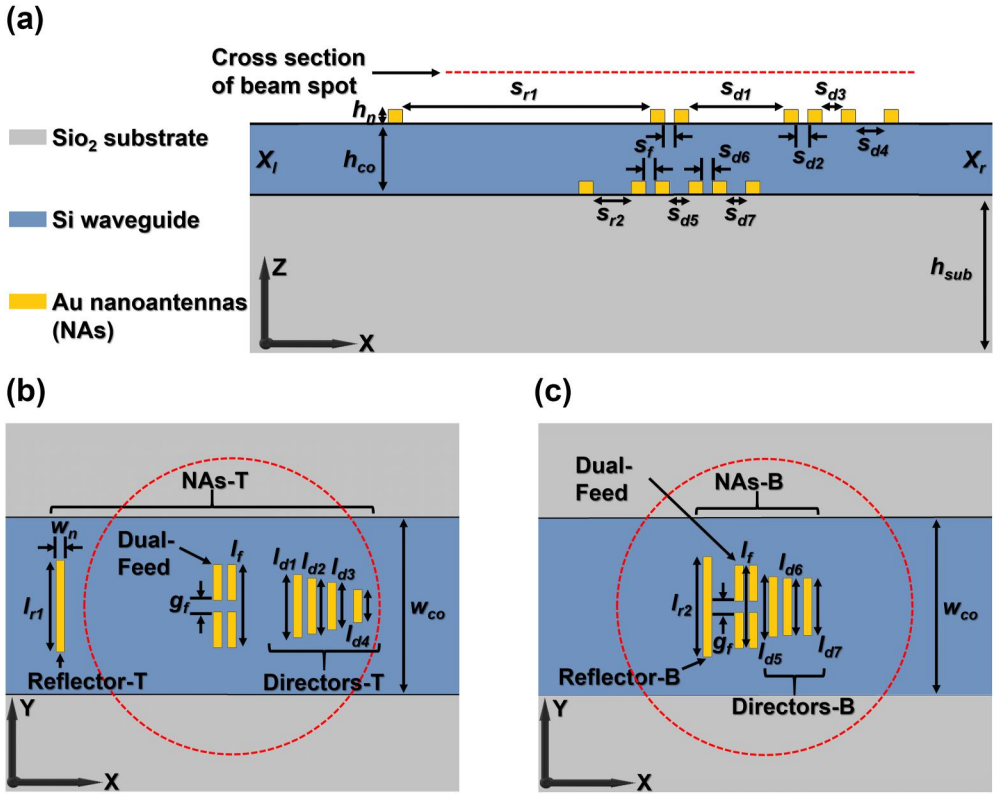

FIGURE 1 Schematic diagram of the two-plane hybrid plasmonic-photonic vertical coupler (HVC), namely 2P-NA HVC. (a) The side view (*XZ* plane), where the two-plane plasmonic nanoantenna (PNA) array (2P-NA) is composed of two different sets of nanoantennas, one of which is placed on the top (NA-T) and the other one at the bottom (NA-B) of the silicon-on-insulator (SOI) waveguide. The dimensions h_n, h_{co}, and h_{sub} are the thicknesses of the Au nanoantenna elements, the SOI waveguide and the SiO_2 substrate, respectively. S_{r1} and S_{r2} are the separations between the reflector and feed at the top and bottom of the waveguide, respectively, and S_{di} (i = 1–7) are the separations between the director elements. X_l and X_r denote the left and right waveguide ports, respectively. (b) The top view (*XY* plane) of the schematic diagram of NA-T. All the Au nanoantenna elements have the same width w_n and the width of the waveguide is w_{co}. The lengths of the feed and reflector elements are l_f and l_{r1} while lengths of the individual director elements are l_{di} (i = 1–4). The gap between the two halves of the feed is denoted by g_f. (c) The top view (*XY* plane) of the schematic diagram for NA-B. The length of the reflector is l_{r2} while the lengths of the individual director elements are l_{di} (i = 5–7). The red dotted line in (a) and cropped circles in (b), (c) are the Gaussian beam positions

we have routinely produced 22-nm gold lines with gaps of 30 nm, which are 25% smaller than the minimum linewidths and gap sizes in this structure. The two-level antennas can be fabricated using a membrane transfer method similar to that used for membrane photonic crystal devices on SOI waveguides [48]. The alignment error of the features within the upper and lower halves of the antenna is limited by the electron beam accuracy within a single write field. The achievable alignment error of the upper and lower layers will be of the order of the minimum feature size and the stitching error between electron beam 'write fields' and is expected to be ~20 nm (<5% of the wavelength of the light inside the silicon waveguide).

Figure 1 shows the device, which is illuminated with a Gaussian beam propagating along the *Z* direction (i.e. from the bottom and through the substrate) with its electric field polarised along the *Y*-axis. The beam is focussed onto the coupler with a beam diameter of 0.8 μm (see Figure 1a).

In the simulations using COMSOL Multiphysics, the vectorial formulation was chosen for the Gaussian beam, which is based on the angular spectrum of plane waves to accurately represent the excitation for reliable calculation of D and PER for large numerical aperture (NA) excitation. The simulation domain was truncated by perfectly matched layers and scattering boundary conditions, and a large simulation domain, 6 μm × 6 μm × 6 μm, was used to further minimise possible reflections off the boundaries.

Figure 2 shows the performance of the 2P-NA HVC. Figure 2a shows CEs to the right and left ports defined as $CE_{r(l)} = 10 \times \log(P_{r(l)}/P_{fp})$, where P_l and P_r are the optical powers at the left X_l and right X_r waveguide ports, respectively (see Figure 1a), and P_{fp} is the total incident optical power at the focus of the excitation beam. According to Figure 2a, coupling efficiencies to the right (CE_r) varies from −8.4 dB to −3.4 dB across the whole 300-nm wavelength range (i.e. 5-dB bandwidth of 300 nm) while CE_l varies from −17.6 to −10.3 dB. As seen in Table 1, the CE is 10x larger and the operating bandwidth is 5x larger than other recently published HVCs. Figure 2b shows D defined as $D = 10 \times \log(P_r/P_l)$, where according to Figure 2b, D varies from 6.4 to 9.2 dB across the ultra-broad wavelength range of 300 nm. Although D varies, it remains above 6.4 dB and is primarily due to a variation in the suppression of the weaker CE_l and, therefore, has minimal impact on the CEr and the detected signal

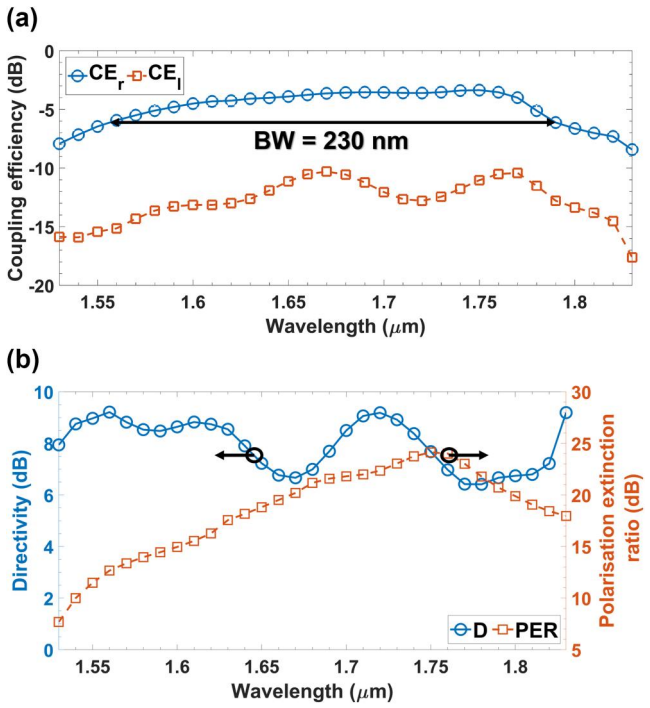

FIGURE 2 The performance of the 2P-NAs hybrid plasmonic-photonic vertical coupler across the telecommunication C- to U-bands for an incident Gaussian beam with a beam diameter of 0.8 μm. (a) Coupling efficiencies to the right (CE_r) and left (CE_l) ports in dB, respectively. (b) Directivity (D) and polarisation extinction ratio (PER) of the 2P-YUPA plasmonic coupler in dB. The black arrows in (b) point each curve to its corresponding *Y*-axis. BW: bandwidth

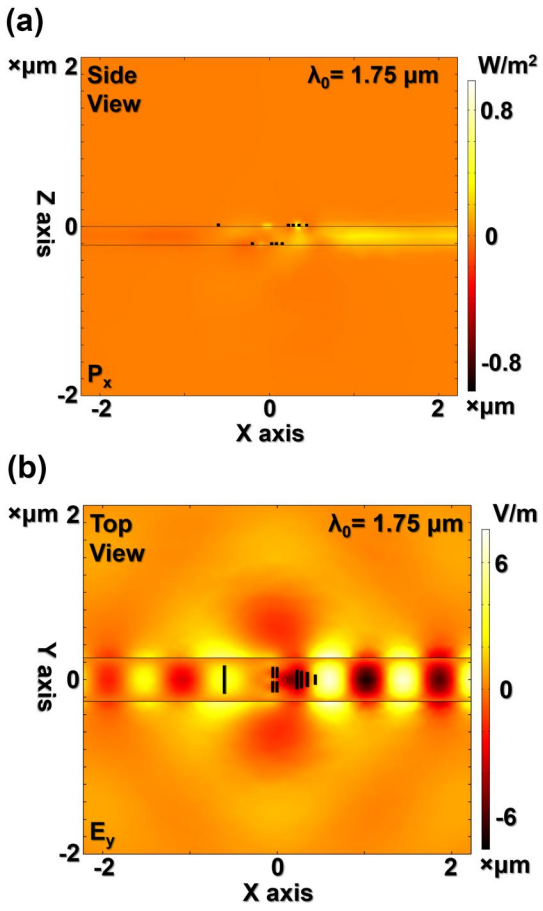

FIGURE 3 Two-dimensional (2D) power and field distributions of the 2P-NA hybrid plasmonic-photonic vertical coupler at a wavelength of $\lambda_0 = 1.75$ μm for an incident Gaussian beam with a beam diameter of 0.8 μm. (a) Side view (i.e. *XZ* plane) of the 2D distribution of the in-plane power flow (P_x). (b) Top view (i.e. *XY* plane) of the 2D field distribution of the *Y*-component of the electric field (E_y)

strength. The fluctuation in D is primarily due to changes in the power coupled in the suppressed direction and not the "coupled" or useful power in the intended signal direction. Since the power in the suppressed direction is very small, small fluctuations have a disproportionately large impact on D. Thus, the fluctuations in D are only important for applications sensitive to power travelling in the suppressed direction (e.g. optical isolation). Figure 2b also shows the PER, defined as $PER = 10 \times \log(P_{r,Y-pol}/P_{r,X-pol})$, where $P_{r,X-pol}$ and $P_{r,Y-pol}$ are the powers at the right port for X- and Y-polarised incident light. The PER varies from 7.7 to 24.1 dB. The polarisation extinction ratio is >10 dB for wavelengths longer than 1.54 μm and the PER is > 20 dB for the 1.66–1.80 μm range. There may be further scope to improve the PER dispersion by adjusting the waveguide geometry to optimise the suppression of the TM_0 mode. This high value of PER illustrates the polarisation-selectivity (purity) of the proposed coupler and make it useful for polarisation-specific applications, such as integrated CARs sensors and polarisation-multiplexed communications with well-defined polarisation orientations. (These structures can also be used to realise polarisation insensitive couplers but their optimisation is different and we defer their consideration to a future paper.) Figure 3 shows both the side view of the 2D distribution of P_x (Figure 3a), the X-component of time-averaged power flow as well as the top view of E_y (Figure 3b), the Y-component of the electric field. These plots illustrate the unidirectional nature of the 2P-NA HVC. Moreover, Figure 3b shows that the dominant mode in the waveguide is TE_0.

As stated, the results in Figures 2 and 3 were obtained for a Gaussian beam diameter of 0.8 μm. This implies that the lens for making such a focal spot needs an NA of 1.4 ($NA \simeq 1.4\ \mu m$ where $\lambda_0 = 1.75\ \mu m$ is the wavelength of the incident light and $r_0 = 0.4\ \mu m$ is the beam radius). Special excitation optics and lenses are needed to achieve the smallest spot sizes. For instance, if the beam angle in the Si substrate exceeds the critical angle of the Si-air interface, the coupling optics will need large NA immersion objectives or lenses etched into the Si substrate (which can be precisely aligned with the coupler during fabrication) [49, 50]. Thus, we examined the impact of larger Gaussian beam diameters, that is, lower NAs, on the performance of the proposed device. The in-coupling efficiency, CE_r, and directivity D are shown in Figure 4 in terms of the Gaussian beam diameter. Figure 4 shows that if the beam diameter is increased to 1.4 μm, the CE_r drops by −3 dB at $\lambda_0 = 1.75$ μm whereas D increases by 1.2 dB. The results imply for an increase of 0.6 μm in the Gaussian beam diameter, the CE_r is still better than −7 dB, that is, more than 20% of the incident light in-couples to the

waveguide, which is very good for a coupler with a wavelength-scale footprint. D increases for larger beam diameters, since more elements of 2P-NA HVC interact with the incoming light and contribute to the multipole interactions, as explained in the next section.

The illumination spot size was fixed to eliminate the impact of a varying spot size (and power density) on the wavelength dependence of the CE. For illumination with a fixed NA lens, Figure 4 shows that the fall off in CE at short wavelengths in Figure 2a would be partially offset by an increase in CE (by ~ 0.5–1 dB) due to the decrease in the spot size at short wavelengths. This also improves the 'flatness' of the CE curve in Figure 2a over the central region between 1.65 and 1.75 μm.

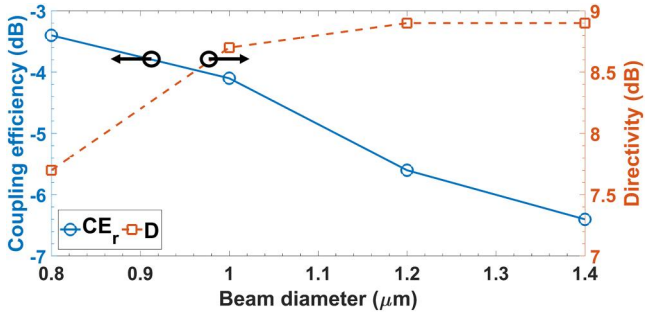

FIGURE 4 The performance of 2P-NA hybrid plasmonic-photonic vertical coupler, coupling efficiencies to the right (CE_r) and D, in terms of the incident Gaussian beam diameter at $\lambda_0 = 1.75$ μm. The black arrows point each curve to its corresponding *Y*-axis

3 | PRINCIPLE OF THE UNIDIRECTIONAL PROPAGATION

The proposed 2P-NA HVC implements an operating principle of the unidirectional propagation function. Along with an electric dipole moment, the 2P-NA supports higher order electric quadrupole and magnetic dipole moments, which are all excited by the incident Gaussian beam. Each of these multipoles has a specific radiation pattern. Figure 5a–c shows the multipole moments of NA-T while Figure 5d–f shows those of the NA-B for a wavelength of $\lambda_0 = 1.75$ μm. Figure 5a,b shows that the director 4, that is, D_4, dominantly supports both electric dipole and quadrupole moments. In the meantime, dual-feed elements, F_T, and the director 3, D_3, of NA-T support a magnetic dipole moment among which the D_3 has the largest magnitude while their magnetic dipole moments are in-phase (see Figure 5c).

According to Figure 5d,e, the F_B, D_6, and D_7 from NA-B support electric dipole and quadrupole moments, where their moments are in-phase relative to each other and the electric moments of D_4 in NA-T. At the same time, the superposition of the magnetic dipole moments of R_B, and D_7 in NA-B resulted in the excitation of the magnetic dipole moment by the NA-B, as shown in Figure 5f. The magnetic dipole moment of NA-B is in-phase to that of NA-T.

By adjusting the lengths of each of the elements of the 2P-NA and aligning their locations with respect to each other, the relative phases of the radiation patterns of the elements can be adjusted to provide unidirectional scattering. In the design of the 2P-NA HVC, the multipoles are adjusted to produce a phase-matched condition on the right-hand side and a phase

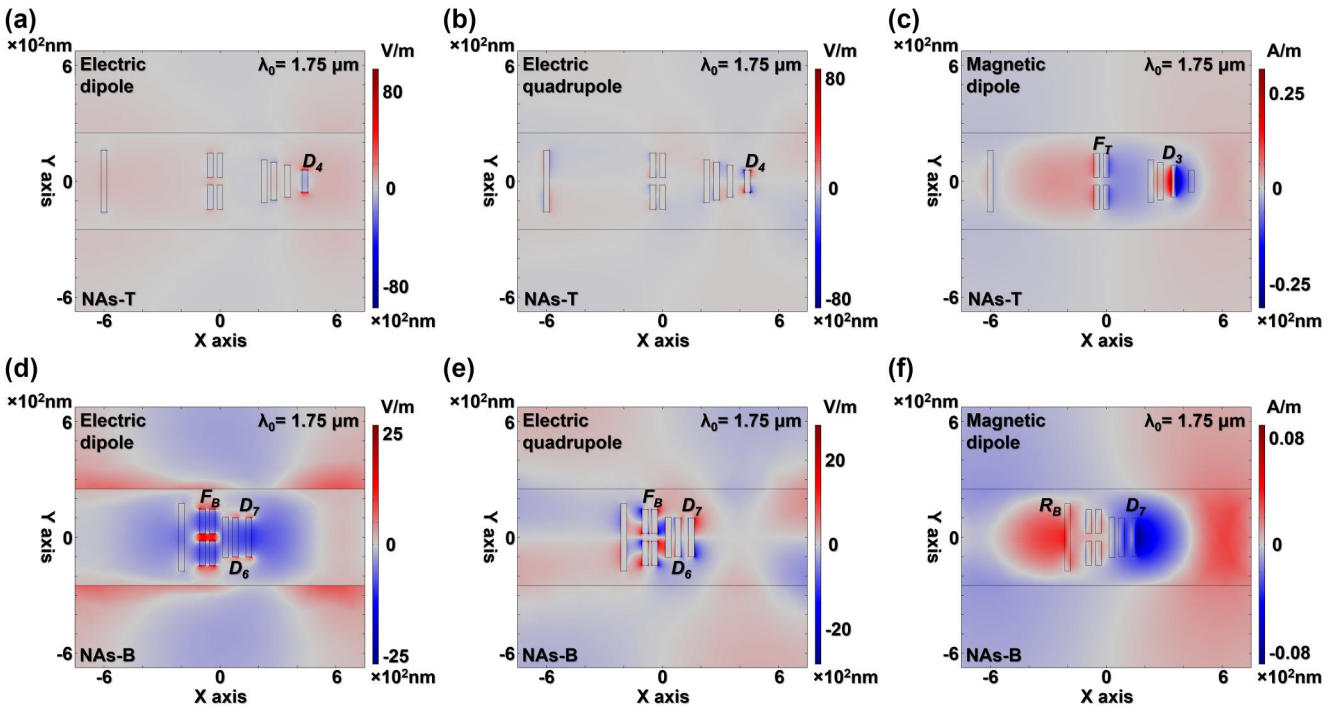

FIGURE 5 Illustration of the 2P-NA hybrid plasmonic-photonic vertical coupler unidirectional propagation principle based on induced multipoles at $\lambda_0 = 1.75$ μm. Electric dipole moment, electric quadrupole moment and magnetic dipole moment of the: (a–c) NA-T, and (d–f) NA-B

mismatch on the left-hand side of the waveguide. The phase match of the fields propagating to the right produces constructive interference of the moments of these multipoles while the phase mismatch results in the destructive interference of the fields propagating to the left. Thus, by coupling the 2P-NA to the evanescent tail of the waveguide mode, the tailored radiation pattern of the multipoles breaks the symmetry of the mode propagation inside the waveguide, forcing the waveguide mode to propagate only along one specific direction. A key innovation of our proposed design is that by adding the second set of nanoantennas, NA-B, we have another degree of freedom to manipulate the interaction of multipoles. In other words, adding NA-B results in an out-of-plane interaction between the multipoles of the 2P-NA elements on the top and bottom of the waveguide. Adjusting and aligning the elements in NA-B relative to those in NA-T brings together out-of-plane and in-plane constructive interferences, improving the overall performance relative to the recently reported HVCs (see Table 1).

4 | OUT-COUPLING PERFORMANCE OF THE DEVICE WITH THE AID OF THE RECIPROCITY THEOREM

According to the reciprocity theorem, an antenna can act as both a receiver and a transmitter. By using the device as a transmitter, or equivalently an out-coupler, we can calculate the far-field radiation pattern of the antenna. When light is incident on the 2P-NA from the substrate side, the in-coupled light propagates towards port X_r (see Figure 3). Thus, the out-coupler here was excited from the right port with a TE_0 waveguide mode. The polar plots for far-field patterns of the effective isotropic radiated power by the 2P-NA (in dB) at $\lambda_0 = 1.75$ μm are shown in the YZ plane at $X = 0$ (Figure 6a) and the XZ plane at $Y = 0$ (Figure 6b). The far-field patterns are normalised to the peak intensity.

The simulation results (see Table 3) show that for a wavelength of $\lambda_0 = 1.75$ μm, slightly more than half of the scattered power, that is, −2.9 dB or 51%, goes towards the substrate whereas −11.5 dB or 7% of the scattered light goes towards the cladding. These values of CEs into the cladding and substrate agree well with the far-field plots (see Figure 6a,b). Thus, the vertical directivity of the out-coupled light is $D_v > 8.5$ dB. The high value of vertical directivity implies that the proposed 2-NA HVC can be used as vertical optical interconnects between two vertically separated circuits. Moreover, at $\lambda_0 = 1.75$ μm, the power reflection is −14.1 dB while the transmission through the waveguide is just −8.7 dB and the power absorbed by the 2P-NA is −6.1 dB. The absorption by the HVC limits the theoretically achievable CE to less than −1.22 dB, but also shows that reducing the transmission past the HVC could increase the CE to −2.0 dB.

5 | CONCLUSION

An ultra-compact (1.07 × 0.62 μm^2) and ultra-broadband (230 nm at 3 dB) HVC is presented that spans the wavelength range of 1.53–1.83 μm. The coupler comprises a unique 2P-NA design that is evanescently coupled to a single-mode SOI waveguide. The design of the coupler takes advantage of dual-feed elements and tailored in- and out-of-plane interference of the 2P-NA multipoles to provide highly efficient unidirectional coupling with high D and PER.

TABLE 3 Out-coupling performance of the 2P-NA HVC

Power loss path	Power loss (dB)	Power loss (%)
Downward emission	−2.9	51
Upward emission	−11.5	7.1
Waveguide through signal	−8.7	13.5
Reflection from 2P-NA HVC	−14.1	3.9
Absorption by 2P-NA HVC	−6.1	24.5

Abbreviation: HVC, hybrid vertical plasmonic-photonic coupler.

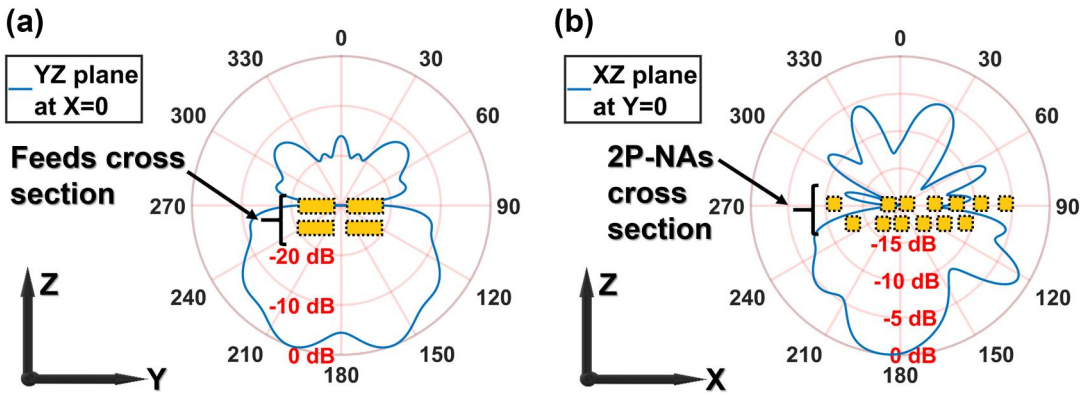

FIGURE 6 Out-coupling performance of the 2P-NA hybrid plasmonic-photonic vertical coupler excited by the TE_0 waveguide mode at $\lambda_0 = 1.75$ μm from port X_r (see Figure 1). (a, b) Polar plots of the far-field patterns of the effective isotropic radiated power in the YZ (at $X = 0$) and XZ planes (at $Y = 0$), normalised to the peak intensity. The gold rectangles depict the cross section of the dual-feed elements of the 2P-NA in (a) and the cross section of the whole 2P-NA in (b). The isopower curves are in dB

Its coupling capability is demonstrated by vertically in-coupling light with a Gaussian beam profile and a diameter of 0.8 μm through the substrate to the TE_0 waveguide mode to give a maximum CE, D, and PER of −3.4 dB, 9.2 dB, and 24.1 dB, respectively. The proposed coupler also acts as a unidirectional out-coupler that provides vertical directivity towards the substrate with $D_v > 8.5$ dB, which can be used as vertical optical interconnects between two vertically separated circuits. Coupling through the substrate improves the CE and makes it possible to excite the coupler with large NA beams (smaller spot size) without the need for immersion objectives and index-matching oil.

We have produced a VC design where the CE of the 2P-NA HVC is > 9 dB higher than that of other ultra-compact PCs and HVCs. The coupler is ideal for vertical coupling of light from optical fibres and VCSEL arrays into high-density PICs for applications in telecommunications, cross-chip communications, such as co-integration with VLSI electronic circuits, and broadband biophotonics. Finally, the high PER, in combination with high D, will also facilitate the simple realisation of polarisation diversified receivers.

ACKNOWLEDGEMENTS

This work was performed in support of research with the Nanoscale and Microscale Research Centre (nmRC), supported by the EPSRC-funded NanoPrime scheme [EP/R025282/1]. Hamed Pezeshki acknowledges the support of a University of Nottingham, Faculty of Engineering Research Excellence scholarship and is grateful to all of those with whom he has had the opportunity to work with. We gratefully acknowledge Dr. Chris Mellor and Dr. Richard Cousins of the nmRC for helpful discussions on fabrication processes.

CONFLICT OF INTEREST

The authors have no conflicts of interest to declare.

DATA AVAILABILITY STATEMENT

The data that support the findings of this study are available from the corresponding author upon reasonable request.

ORCID

Hamed Pezeshki https://orcid.org/0000-0001-8252-0525

REFERENCES

1. Pu, M.H., et al.: Ultra-low-loss inverted taper coupler for silicon-on-insulator ridge waveguide. Opt. Commun. 283(19), 3678–3682 (2010)
2. Sanchez-Postigo, A., et al.: Broadband fiber-chip zero-order surface grating coupler with 0.4 dB efficiency. Opt. Lett. 41(13), 3013–3016 (2016)
3. Tong, Y.Y., Zhou, W., Tsang, H.K.: Efficient perfectly vertical grating coupler for multi-core fibers fabricated with 193 nm DUV lithography. Opt. Lett. 43(23), 5709–5712 (2018)
4. Lopez-Tejeira, F., et al.: Efficient unidirectional nanoslit couplers for surface plasmons. Nat. Phys. 3(5), 324–328 (2007)
5. Taminiau, T.H., Stefani, F.D., van Hulst, N.F.: Enhanced directional excitation and emission of single emitters by a nano-optical Yagi-Uda antenna. Opt. Express. 16(14), 10858–10866 (2008)
6. Alu, A., Engheta, N.: Wireless at the nanoscale: optical interconnects using matched nanoantennas. Phys. Rev. Lett. 104(21) (2010)
7. Koenderink, A.F.: Plasmon nanoparticle array waveguides for single photon and single plasmon sources. Nano Lett. 9(12), 4228–4233 (2009)
8. Kosako, T., Kadoya, Y., Hofmann, H.F.: Directional control of light by a nano-optical Yagi-Uda antenna. Nat. Photonics. 4(5), 312–315 (2010)
9. Curto, A.G., et al.: Unidirectional emission of a quantum dot coupled to a nanoantenna. Science. 329(5994), 930–933 (2010)
10. Maksymov, I.S., et al.: Optical Yagi-Uda nanoantennas. Nanophotonics. 1(1), 65–81 (2012)
11. Ho, J., et al.: Highly directive hybrid metal–dielectric Yagi-Uda nanoantennas. ACS Nano. 12(8), 8616–8624 (2018)
12. Baehr-Jones, T., et al.: Myths and rumours of silicon photonics. Nat. Photonics. 6(4), 206–208 (2012)
13. Rodriguez-Fortuno, F.J., Espinosa-Soria, A., Martinez, A.: Exploiting metamaterials, plasmonics and nanoantennas concepts in silicon photonics. J. Opt. 18(12) (2016)
14. Trinh, P.D., et al.: Silicon-on-Insulator (SOI) phased-array wavelength multi/demultiplexer with extremely low-polarization sensitivity. IEEE Photon. Technol. Lett. 9(7), 940–942 (1997)
15. Horst, F., et al.: Cascaded mach-zehnder wavelength filters in silicon photonics for low loss and flat pass-band wdm (de-) multiplexing. Opt. Express. 21(10), 11652–11658 (2013)
16. Marchetti, R., et al.: Coupling strategies for silicon photonics integrated chips [invited]. Photon. Res. 7(2), 201–239 (2019)
17. Nambiar, S., Sethi, P., Selvaraja, S.: Grating-assisted fiber to chip coupling for SOI photonic circuits. Appl. Sci. 8(7), 1142 (2018)
18. Xiao, Z., et al.: Bandwidth analysis of waveguide grating coupler. Opt Express. 21(5), 5688–5700 (2013)
19. Andryieuski, A., Lavrinenko, A.V.: Nanocouplers for infrared and visible light. Adv. Optoelectron. 2012 (2012). https://doi.org/10.1155/2012/839747
20. Subbaraman, H., et al.: Recent advances in silicon-based passive and active optical interconnects. Opt. Express. 23(3), 2487–2510 (2015)
21. Ayata, M., et al.: Compact, ultra-broadband plasmonic grating couplers. Opt Express. 27(21), 29719–29729 (2019)
22. Vlasov, Y.A., McNab, S.J.: Losses in single-mode silicon-on-insulator strip waveguides and bends. Opt. Express. 12(8), 1622–1631 (2004)
23. Dumon, P., et al.: Low-loss SOI photonic wires and ring resonators fabricated with deep UV lithography. IEEE Photon. Technol. Lett. 16(5), 1328–1330 (2004)
24. Tsilipakos, O., et al.: Interfacing dielectric-loaded plasmonic and silicon photonic waveguides: theoretical analysis and experimental demonstration. IEEE J. Quant. Electron. 48(5), 678–687 (2012)
25. Emboras, A., et al.: Efficient coupler between silicon photonic and metal-insulator-silicon-metal plasmonic waveguides. Appl. Phys. Lett. 101(25), 251117 (2012)
26. Dasgupta, A., et al.: Directional fluorescence emission mediated by chemically-prepared plasmonic nanowire junctions. J. Phys. Chem. C. 120(31), 17692–17698 (2016)
27. Li, H.B., et al.: Directional emission of surface-enhanced Raman scattering based on a planar-film plasmonic antenna. Thin Solid Films. 520(18), 6001–6006 (2012)
28. Dorfmuller, J., et al.: Near-field dynamics of optical Yagi-Uda nanoantennas. Nano Lett. 11(7), 2819–2824 (2011)
29. Nikoufard, M., Nourmohammadi, A., Esmaeili, S.: Hybrid plasmonic nanoantenna with the capability of monolithic integration with laser and photodetector on InP substrate. IEEE Trans. Antenn. Propag. 66(1), 3–8 (2017)
30. Bellanca, G., et al.: Integrated Vivaldi plasmonic antenna for wireless on-chip optical communications. Opt. Express. 25(14), 16214–16227 (2017)
31. Bernal Arango, F., Kwadrin, A., Koenderink, A.F.: Plasmonic antennas hybridized with dielectric waveguides. ACS Nano. 6(11), 10156–10167 (2012)
32. Obelleiro, F., et al.: Directive antenna nanocoupler to plasmonic gap waveguides. Opt. Lett. 38(10), 1630–1632 (2013)
33. Lin, J., et al.: Polarization-controlled tunable directional coupling of surface plasmon polaritons. Science. 340(6130), 331–334 (2013)

34. Guo, R., et al.: Bidirectional waveguide coupling with plasmonic fano nanoantennas. Appl. Phys. Lett. 105(5) (2014)
35. Guo, R., et al.: High-bit rate ultra-compact light routing with mode-selective on-chip nanoantennas. Sci. Adv. 3(7) (2017)
36. Strzelecka, E.M., et al.: Parallel free-space optical interconnect based on arrays of vertical-cavity lasers and detectors with monolithic microlenses. Appl. Opt. 37(14), 2811–2821 (1998)
37. Khurgin, J.B., Sun, G.: Comparative analysis of spasers, vertical-cavity surface-emitting lasers and surface-plasmon-emitting diodes. Nat. Photonics. 8(6), 468–473 (2014)
38. McPolin, C.P., et al.: Integrated plasmonic circuitry on a vertical-cavity surface-emitting semiconductor laser platform. Nat. Commun. 7(1), 1–8 (2016)
39. Krishnamoorthy, A.V., et al.: Computer systems based on silicon photonic interconnects. Proc. IEEE. 97(7), 1337–1361 (2009)
40. Apsel, A., Pappu, A., Yin, T.: Merging traditional VLSI with photonics. In: Proceedings of the lightwave technologies in instrumentation and measurement conference. IEEE, Palisades 2004 (2004)
41. Beausoleil, R.G., et al.: Nanoelectronic and nanophotonic interconnect. Proc. IEEE. 96(2), 230–247 (2008)
42. Savidis, I., et al.: Heterogeneous 3-D circuits: integrating free-space optics with cmos. Microelectron. J. 50, 66–75 (2016)
43. Yampolsky, S., et al.: Seeing a single molecule vibrate through time-resolved coherent anti-Stokes Raman scattering. Nat. Photonics. 8(8), 650–656 (2014)
44. Steuwe, C., et al.: Surface enhanced coherent anti-Stokes Raman scattering on nanostructured gold surfaces. Nano Lett. 11(12), 5339–5343 (2011)
45. Kischkat, J., et al.: Mid-infrared optical properties of thin films of aluminum oxide, titanium dioxide, silicon dioxide, aluminum nitride, and silicon nitride. Appl. Opt. 51(28), 6789–6798 (2012)
46. Pierce, D.T., Spicer, W.E.: Electronic-structure of amorphous Si from photoemission and optical studies. Phys. Rev. B. 5(8), 3017–3029 (1972)
47. Johnson, P.B., Christy, R.W.: Optical constants of the noble metals. Phys. Rev. B. 6(12) (1972)
48. Crosnier, G., et al.: High Q factor InP photonic crystal nanobeam cavities on silicon wire waveguides. Opt. Lett. 41(3), 579–582 (2016)
49. Strzelecka, E., et al.: Monolithic integration of vertical-cavity laser diodes with refractive GaAs microlenses. Electron. Lett. 31(9), 724–725 (1995)
50. Strzelecka, E., et al.: Fabrication of refractive microlenses in semiconductors by mask shape transfer in reactive ion etching. Microelectron. Eng. 35(1–4), 385–388 (1997)

How to cite this article: Pezeshki, H., Wright, A.J., Larkins, E.C.: Ultra-compact and ultra-broadband hybrid plasmonic-photonic vertical coupler with high coupling efficiency, directivity, and polarisation extinction ratio. IET Optoelectron. 1–9 (2021). https://doi.org/10.1049/ote2.12063